

Top quark anomalous tensor couplings in the two-Higgs-doublet models

Lucía Duarte,^a Gabriel A. González-Sprinberg^b and Jordi Vidal^{c,d}

^a*Instituto de Física, Facultad de Ingeniería, Universidad de la República, Julio Herrera y Reissig 565, Montevideo 11000, Uruguay*

^b*Instituto de Física, Facultad de Ciencias, Universidad de la República, Iguá 4225, Montevideo 11600, Uruguay*

^c*Departament de Física Teòrica Universitat de València, Dr. Moliner 50, E-46100 Burjassot, València, Spain*

^d*Instituto de Física Corpuscular (IFIC), Centro Mixto Universitat de València-CSIC, València, Spain*

E-mail: lucia@fisica.edu.uy, gabrielg@fisica.edu.uy, vidal@uv.es

ABSTRACT: We compute the one loop right and left anomalous tensor couplings (g_R and g_L , respectively) for the top quark, in the aligned two-Higgs-doublet model. They are the magnetic-like couplings in the most general parameterization of the tbW vertex. We find that the aligned two-Higgs doublet model, that includes as particular cases some of the most studied extensions of the Higgs sector, introduces new electroweak contributions and provides theoretical predictions that are very sensitive to both new scalar masses and the neutral scalar mixing angle. For a large area in the parameters space we obtain significant deviations in both the real and the imaginary parts of the couplings g_R and g_L , compared to the predictions given by the electroweak sector of the Standard Model. The most important ones are those involving the imaginary part of the left coupling g_L and the real part of the right coupling g_R . The real part of g_L and the imaginary part of g_R also show an important sensitivity to new physics scenarios. The model can also account for new CP violation effects via the introduction of complex alignment parameters that have important consequences on the values for the imaginary parts of the couplings. The top anomalous tensor couplings will be measured at the LHC and at future colliders providing a complementary insight on new physics, independent from the bounds in top decays coming from B physics and $b \rightarrow s\gamma$.

KEYWORDS: Beyond Standard Model, Standard Model

Contents

1	Introduction	1
2	A2HDM: overview	2
3	Top tensor couplings in the A2HDM	4
3.1	Observables and experimental status	5
3.2	Our calculation	6
4	Results	8
4.1	Contributions to g_R	9
4.2	Contributions to g_L	12
4.3	Contributions from Type I and II 2HDM	15
5	Conclusions	16

1 Introduction

The recent discovery at the LHC of a new neutral boson [1, 2] points to a spontaneous electroweak symmetry breaking mechanism involving scalars, but more experimental analyses are still needed to distinguish whether we face the unique Standard Model (SM) Higgs boson or an extended scalar sector. Besides, top quark physics at the LHC can play a role in this quest, as it is expected to probe physics beyond the electroweak scale.

While no deviation from the SM predictions has been found in top physics yet [3–6], the angular distribution in the dominant decay mode $t \rightarrow bW^+$ is going to be precisely measured at the LHC. This measurement can probe the SM beyond tree-level and might be sensitive to new physics in the electroweak sector, where it is expected to appear. Besides, new physics interactions might show up in the measurements of the top anomalous couplings because they may modify the strength and structure of the tbW vertex. The SM one loop predictions for the anomalous tensor couplings receive contributions from QCD, coming from gluon exchange, and from the electroweak (EW) sector of the SM. The real parts of the couplings receive contributions from both QCD and the EW sectors, while the imaginary parts are generated exclusively by the EW corrections. The electroweak contributions to the right and left top anomalous tensor couplings, g_R and g_L respectively, have recently been calculated in ref. [7, 8]. These quantum corrections amount to 19% of the dominant QCD contribution for the real part of the right coupling g_R , and 9% for the real part of the left coupling g_L . This last prediction is in slight tension with existing indirect constraints obtained recently from B decays data [9, 10]. Besides, in ref. [7, 8] the imaginary parts of g_R and g_L and the real part of g_L were also calculated. Direct

constraints on the top anomalous couplings were obtained by D0 [3] at Tevatron, and by ATLAS and CMS [4–6] at the LHC. These last are still looser than the indirect ones, but a much better sensitivity is expected in the LHC measurements in the future [11].

Among the SM extensions, the inclusion of one extra scalar doublet is a minimal choice and results in a variety of dynamical possibilities. Two-Higgs-doublet models (2HDM) can also be read as a low energy effective theory. Besides, they provide new ways to introduce CP violation sources, both in the scalar potential and in the Yukawa sector. Many new physics scenarios, including supersymmetry, can lead to a low energy spectrum containing the SM fields, plus additional scalar multiplets. In general, 2HDMs allow the appearance of unwanted flavor changing neutral currents (FCNCs) unless ad-hoc restrictions are imposed at the lagrangian, such as \mathcal{Z}_2 symmetries that, in addition, also forbid CP violation in the scalar potential. These so-called natural flavor conservation models include the well known types I, II, III, X, Y and the inert 2HDM. For a comprehensive review see [12]. A less restrictive and more general alternative is given by the aligned two-Higgs-doublet model (A2HDM) [13], which imposes the proportionality of both Yukawa matrices, with complex alignment parameters, and includes all the previously mentioned models as particular limits. These complex alignment parameters allow for a new CP violation source in the Yukawa sector, independently of the form of the potential, and in addition to the Cabibbo-Kobayashi-Maskawa quark mixing matrix.

Previous works have studied the top quark decay vertex in the context of the 2HDM (type II), the MSSM, little Higgs and TC2 models [14–16]. In this paper we calculate the top quark anomalous tensor couplings in the general framework of the A2HDM. Our work complements the flavor physics analysis where this model has been thoroughly studied [17–20], and the recent work [21] that takes into account the LHC measurements.

In section 2 we briefly review the A2HDM and comment on the constraints for its parameters. In section 3 we define the vertex parameterization and, in section 3.1, we review the theoretical and experimental status of the top anomalous tensor couplings. Our analytical calculation is introduced in section 3.2 and numerical results for the different scalars mass scenarios chosen is presented in section 4. In particular, we compare the A2HDM predictions for the top anomalous tensor couplings to the recently calculated electroweak values. We investigate the sensitivity of the anomalous tensor couplings (g_R in section 4.1 and g_L in section 4.2) to the scalars mixing angle and alignment parameters, taking a CP conserving scalar potential, but allowing the presence of complex CP violating phases. The results for the Type I and II 2HDM are also shown in section 4.3. Finally, we present our conclusions in section 5.

2 A2HDM: overview

The 2HDMs extend the SM by adding a second scalar doublet of hypercharge $Y=1/2$. The EW sector in these models is significantly different from the SM. The A2HDM model incorporates, in addition to three Goldstone bosons, five physical scalars: two charged scalar fields $H^\pm(x)$ and three neutral scalars $\{\varphi_i(x)\}_{i=1,2,3} = \{h(x), H(x), A(x)\}$, related

through an orthogonal transformation \mathcal{R} to the gauge eigenstates S_i :

$$\varphi_i(x) = \mathcal{R}_{ij} S_j(x); \quad i, j = 1, 2, 3. \quad (2.1)$$

The mixing matrix \mathcal{R} depends on the particular form of the potential, which is also responsible of the structure of the scalars mass matrix and mass eigenstates. Taking a CP conserving potential and in the so-called Higgs basis, where only one doublet acquires a nonzero vacuum expectation value, the mixing matrix is written as:

$$\begin{pmatrix} H \\ h \\ A \end{pmatrix} = \begin{pmatrix} \cos \gamma & \sin \gamma & 0 \\ -\sin \gamma & \cos \gamma & 0 \\ 0 & 0 & 1 \end{pmatrix} \begin{pmatrix} S_1 \\ S_2 \\ S_3 \end{pmatrix}, \quad (2.2)$$

where γ is the neutral scalars mixing angle.

The generic Yukawa lagrangian, with standard fermionic content, gives rise to FCNCs because the Yukawa couplings of both doublets cannot be simultaneously diagonalized. Tree-level FCNCs can be avoided by requiring the *alignment* in flavor space of the Yukawa couplings, i.e., by making both Yukawa matrices to be proportional to each other, for each type of right handed fermion. If, in addition, the proportionality parameters ς_f ($f \equiv u, d, l$) are taken to be arbitrary complex numbers then new sources of CP violation are introduced.

In the mass eigenstates basis the Yukawa lagrangian is written as:

$$\begin{aligned} \mathcal{L}_Y = & -\frac{\sqrt{2}}{v} H^+(x) \bar{u}(x) [\varsigma_d V M_d P_R - \varsigma_u M_u V P_L] d(x) \\ & -\frac{\sqrt{2}}{v} H^+(x) \varsigma_l \bar{\nu}(x) M_l P_R l(x) \\ & -\frac{1}{v} \sum_{i,f} \varphi_i(x) y_f^{\varphi_i} \bar{f}(x) M_f P_R f(x) + h.c., \end{aligned} \quad (2.3)$$

where V is the Cabibbo-Kobayashi-Maskawa matrix, $P_{R,L} \equiv \frac{1}{2}(1 \pm \gamma_5)$ are the chirality projectors and M_f ($f \equiv u, d, l$) are the diagonal mass matrices.

The neutral Yukawa terms are flavor-diagonal and the couplings $y_f^{\varphi_i}$ are proportional to the corresponding elements of the neutral scalar mixing matrix \mathcal{R} :

$$y_{d,l}^{\varphi_i} = \mathcal{R}_{i1} + (\mathcal{R}_{i2} + i\mathcal{R}_{i3})\varsigma_{d,l}, \quad y_u^{\varphi_i} = \mathcal{R}_{i1} + (\mathcal{R}_{i2} - i\mathcal{R}_{i3})\varsigma_u^*. \quad (2.4)$$

The A2HDM leads to a structure where all fermion-scalar interactions are proportional to the fermion masses, giving rise to a hierarchy of non tree-level FCNC effects. Bounds on the ς_f parameters have been explored in ref. [17], in the context of charged Higgs phenomenology. There, constraints on the $\varsigma_{u,d,l}$ parameters as a function of m_{H^\pm} were obtained from lepton decays and leptonic and semi-leptonic tree-level decays of pseudoscalar mesons. From tau decays they obtained that $|\varsigma_l|/m_{H^\pm} \leq 0.40 \text{ GeV}^{-1}$ and from a global fit to leptonic and semi-leptonic decays they got the bounds $|\varsigma_u \varsigma_l^*|/m_{H^\pm}^2 \lesssim 0.01 \text{ GeV}^{-2}$ and $|\varsigma_d \varsigma_l^*|/m_{H^\pm}^2 < 0.1 \text{ GeV}^{-2}$

Bounds on $|\varsigma_u|$, obtained from the top quark loops contributions in $Z \rightarrow b\bar{b}$ decays, give $|\varsigma_u| < 0.91(1.91)$ for $m_{H^\pm} = 80(500) \text{ GeV}$ [17]. Mixing processes, such as $B^0 - \bar{B}^0$ and

$K^0 - \bar{K}^0$ mixing, result in less restrictive limits because they depend on the relative phase between the alignment parameters ς_u and ς_d . From the radiative decay $\bar{B} \rightarrow X_s \gamma$, the bound $|\varsigma_u| |\varsigma_d| \lesssim 20$, for $M_{H^\pm} \in (80, 500)$ GeV, is obtained by assuming $|\varsigma_u| < 3$ [17]. More recently, the observed excess in τ lepton production in semileptonic B-meson decays reported by BaBar [22] has been analyzed within the A2HDM context and it points towards bigger values for the product $|\varsigma_l^* \varsigma_u|/m_{H^\pm}$ than the one previously obtained in ref. [20]. A recent paper [21] analyzes the A2HDM in the light of the ‘‘Higgs-like’’ particle discovery [1, 2] and Higgs signals data from Tevatron [23] getting some constraints even with the large experimental uncertainties existing up to now. The authors search for possible ways to enhance the diphoton channel while being compatible with the rest of the data. Although a pure CP-odd assignment for the new particle is ruled out, they investigate several possibilities including the CP conserving \mathcal{Z}_2 limit, degenerate CP violating mixtures in the scalar potential and charged scalars contributions to the amplitude $h \rightarrow 2\gamma$. Concerning the A2HDM an enhancement is obtained in the $\gamma\gamma$ rate with a complex top Yukawa coupling with real part close to the SM value.

3 Top tensor couplings in the A2HDM

The tbW^+ vertex can be studied by parameterizing the amplitude \mathcal{M}_{tbW} of the $t(p) \rightarrow b(p')W^+(q)$ decay with the most general Lorentz structure, for on-shell particles, in the following way:

$$\mathcal{M}_{tbW} = -\frac{e}{\sin \theta_w \sqrt{2}} \epsilon^{\mu*} \times \bar{u}_b(p') \left[\gamma_\mu (V_L P_L + V_R P_R) + \frac{i \sigma_{\mu\nu} q^\nu}{M_W} (g_L P_L + g_R P_R) \right] u_t(p), \quad (3.1)$$

where the outgoing W^+ momentum, mass and polarization vector are $q = p - p'$, M_W and $\epsilon^{\mu*}$, respectively. The form factors are all dimensionless; V_L and V_R parameterize the vector and axial-vector couplings while g_L and g_R are the so called left and right anomalous tensor couplings, respectively.

The expression (3.1) is the most general model independent parameterization for the tbW^+ vertex. Another approach to the problem is the effective lagrangian method. This technique describes the low energy physics of a theory by using non-renormalized terms in the lagrangian written with the SM fields and invariant under the gauge symmetry of the SM. This approach assumes that the new physics spectrum is very well above the EW energy scale [24–26]. In this paper we will adopt the first approach that does not rely on any particular assumptions and that it is compatible with the energy scales explored by the LHC.

The tree level SM values for the couplings are $V_L = V_{tb}$ and $V_R = g_R = g_L = 0$. All these couplings receive corrections at one loop in the SM and in extended models. The measurement of $V_L = V_{tb} \simeq 1$ is still affected by large uncertainties [27] and its determination may be an open window to test new physics, but this issue and any possible deviations of V_R from 0 will not be the target of this work, where we concentrate only on the tensor couplings g_R and g_L .

Within the SM, the dominant contribution to the real part of the tensor couplings comes from the QCD one loop diagram, generated by gluon exchange. The computed values for g_R^{QCD} [28] and for g_L^{QCD} [7, 8], for $m_t = 171$ GeV, are:

$$g_R^{QCD} = -6.61 \times 10^{-3}, \quad g_L^{QCD} = -1.118 \times 10^{-3}. \quad (3.2)$$

Both the real and the imaginary one loop corrections in the EW sector for the SM were obtained in ref. [7, 8] for a SM Higgs h^0 with $m_{h^0} = 150$ GeV. The values of the electroweak contribution to these couplings in the SM but for the now measured value $m_{h^0} = 126$ GeV are:

$$g_R^{EW} = -(1.24 + 1.23i) \times 10^{-3}, \quad g_L^{EW} = -(0.102 + 0.014i) \times 10^{-3}. \quad (3.3)$$

The imaginary numbers come exclusively from absorptive parts in some of the EW diagrams. The complete SM one loop contributions, including the one loop QCD and the electroweak SM contributions for the tensor couplings are then:

$$g_R^{SM} = -(7.85 + 1.23i) \times 10^{-3}, \quad g_L^{SM} = -(1.220 + 0.014i) \times 10^{-3}. \quad (3.4)$$

From eqs. (3.3) and (3.4) it can be seen that for the real part of g_R and g_L , the EW contribution is 16% and 8%, respectively, of the total SM values. To be sensitive to new physics in the real part of the couplings, one has to be accurate enough in the measurement to disentangle the QCD and EW contributions. Instead, the imaginary parts are directly sensitive to new physics, because they come only from the EW diagrams. Note that the imaginary right coupling is of the same order of magnitude than the real parts of both couplings; however, for the left coupling, the imaginary part is very small. Because the anomalous tensor couplings are chirality flipping quantities, the EW contributions to g_L are lower in magnitude than those for g_R , due to the flow of chirality in the diagrams with the standard tbW vertex.

3.1 Observables and experimental status

Besides the observables that were already considered in the literature -branching ratios, helicity fractions, angular distributions and asymmetries [29, 30]- new observables have been defined in ref. [11]. These make use of the spin properties of the polarized top quarks produced at the LHC in order to define quantities that are sensitive to the imaginary parts of the anomalous tensor couplings. The imaginary part of the anomalous tensor couplings is not a CP-odd quantity, but CP violation can nevertheless be investigated by comparing the properties of the top and anti-top decay vertex: a change in the sign of the imaginary parts of the decay tensor couplings ($Im(g_R)$ and/or $Im(g_L)$), when comparing top and anti-top, would point out to CP violation.

The normal asymmetry A_{FB}^N , defined in [11], considers the orthogonal direction to the plane defined by the top spin and the W momenta. The forward and backward directions are defined with respect to the angle of the charged lepton (into which the W decays) momenta in the W rest frame with the W momenta in the top rest frame. This asymmetry vanishes for real anomalous couplings and, consequently, it turns out to be very sensitive

to $Im(g_R)$. For small g_R and taking $V_L = 1$, $V_R = g_L = 0$, the authors obtain $A_{FB}^N = 0.64 \cdot P \cdot Im(g_R)$, for top quarks with normal polarization degree P . A combined analysis of this new observable together with the usual W helicity fractions, the asymmetries in the top quark rest frame, and the tW cross section, allows a model independent fit of all the tbW vertex parameters [11, 31]. Preliminary measurements of the normal forward-backward asymmetry using data up to 2011 at the LHC give the bound $-0.07 \leq Im(g_R) \leq 0.18$ at 68% CL [6].

ATLAS and CMS have recently published bounds for the top anomalous couplings. They analyzed data obtained in 2010 and 2011 on the W helicity fractions in top pair events. The CMS bounds [5] are given in two different scenarios: (i) assuming $V_L = 1, V_R = g_L = 0$ and leaving $Re(g_R)$ as a free parameter, and (ii) leaving V_R to be free. The first assumption (i) gives the best fitted value: $Re(g_R) = -0.008 \pm 0.024(stat.)_{-0.030}^{+0.029}(syst.)$. ATLAS limits $-0.14 < Re(g_L) < 0.11$ and $-0.08 < Re(g_R) < 0.04$, at 95% CL [4], were obtained assuming all anomalous couplings set to zero, except the one to be bounded.

Direct bounds for the top anomalous couplings are also available from Tevatron. D0 Collaboration [32] performed a combined analysis of the measurements of the W bosons helicities [3] and those of the single top quark production [33]. Taking real anomalous form factors, they studied the allowed regions of the squared modulus of a form factor, $|g_{L,R}|^2$ or, alternatively, $|V_R|^2$, as a function of $|V_L|^2$ with all other couplings set to zero. A different analysis of early LHC data can be found in ref. [34] where they combined recent measurements in ATLAS of top quark decay asymmetries with the t-channel single top cross section measured by CMS. This combination of data allows a better determination of the anomalous couplings bounds: they plotted the allowed regions in the (g_L, g_R) plane at 95% CL, assuming $V_L = 1, V_R = 0$ and that both tensor couplings are real, resulting in the limits $|g_L| \leq 0.45$, and $-0.55 \leq g_R \leq 0.20$ or $0.70 \leq g_R \leq 0.90$.

Finally, indirect bounds were obtained [9, 10] from the $Br(B \rightarrow X_s \gamma)$ branching ratio, measured at B factories. These last results use the most recent global fits in neutral mesons oscillations [35, 36] and represent the strongest bounds on the anomalous tensor couplings. In our notation, they get the following bounds: $-0.001 < Re(g_L) < 0.0003$ and $-0.07 < Re(g_R) < 0.27$, at 95% CL, assuming real couplings, $V_L = 1$ and only one non-vanishing form factor at a time.

3.2 Our calculation

Let us start discussing the general features of the $t \rightarrow bW^+$ decay in the A2HDM. We will concentrate in the EW part because it is the only one that is different from the SM.

At tree-level the fermion couplings to gauge bosons are not modified with respect to the SM by the presence of a new scalar doublet, so that the tbW vertex remains unchanged. However, at one loop, besides the SM fields (top and bottom quarks, gluons, gauge bosons W, Z and γ , and Goldstone bosons $G^{0\pm}$), we have to consider the contributions of the new fields (the three neutral scalars h, H and A , and the charged scalars H^\pm) circulating in the internal lines of the loop.

There is only one topology of the one loop diagrams that contributes to the vertex and, thus, to the anomalous tensor couplings. This is shown in figure 1.

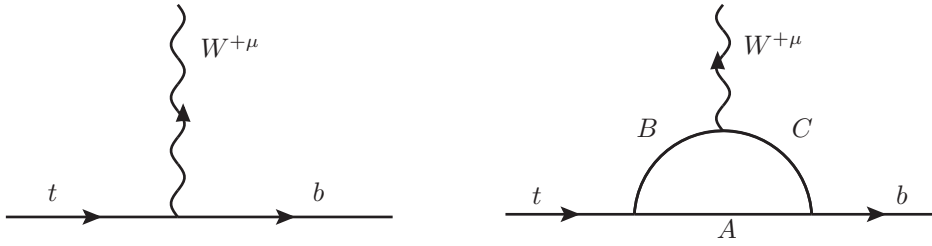


Figure 1. The $t \rightarrow bW^+$ vertex: tree-level and one loop diagrams.

Type	Particles in the loop ABC
(a)	$\varphi_i t b$
(b)	$t \varphi_i H^+$
(c)	$b H^+ \varphi_i$
(d)	$t \varphi_i G^+$
(e)	$b G^+ \varphi_i$
(f)	$t \varphi_i W^+$
(g)	$b W^+ \varphi_i$

Table 1. Classification of the Feynman diagrams by the type of particles circulating in the loop

The different Feynman diagrams in the calculation are identified by naming the particles circulating in the loop as ABC . We show in table 1 the diagrams classified by the position taken by the neutral scalars φ_i : in type (a) the neutral scalars take position A, in (b), (d) and (f) they are in position B, with a t quark in the loop, and in (c), (e) and (g) they are in position C, with a b quark in the loop. Depending on the value for the mass of the charged scalar H^+ , diagrams type (c) can develop absorptive parts. In addition, diagrams type (e) and (g) always have an imaginary part.

We recover the SM values from the A2HDM just taking the $m_{H,A,H^+} \rightarrow \infty$ limit and identifying $h \equiv h^0$. In that limit we explicitly checked that the contributions to the anomalous tensor form factors in the A2HDM are identical to the EW corresponding ones obtained in [7, 8]. These are the (a), (d), (e), (f) and (g) diagrams, where we set $\gamma = -\pi/2$ in such a way that the neutral scalar h has the same couplings as the SM Higgs boson.

The vertices that contribute to the top anomalous tensor couplings in the A2HDM depend on the scalar mixing angle γ and on the alignment parameters ς_u and ς_d . The mass dependence is parameterized by the dimensionless variable $r_X = m_X/m_t$, where m_X is the mass of the particle X circulating in the loop. For the neutral scalar masses above the TeV scale the Feynman integrals give negligible values when compared to the EW contributions. However, there is a high sensitivity of the tensor couplings on the masses of the new particles when they take lower values.







Scalar mass scenarios (in GeV)		
I	$m_h = 126, m_H = 173, m_A = 150, m_{H^+} = 320$	
Ii	$m_h = 126, m_H = 173, m_A = 150, m_{H^+} = 150$	
II	$m_h = 126, m_H = 865, m_A = 865, m_{H^+} = 320$	
IIi	$m_h = 126, m_H = 865, m_A = 865, m_{H^+} = 150$	
III	$m_h = 865, m_H = 865, m_A = 126, m_{H^+} = 320$	
IIIi	$m_h = 865, m_H = 865, m_A = 126, m_{H^+} = 150$	

Table 2. Different scalar mass scenarios taken for the analysis. Each scenario is identified by a different color and type of line. All masses are in GeV.

4 Results

In this section we show the results of our calculation for the top anomalous magnetic moments in the A2HDM. As already stated, the model introduces new physics only in the EW sector. To explicitly show the size of these corrections to the EW sector of the SM, we will compare the new contributions from the A2HDM with the values one gets from the EW contribution of the SM (SM-EW). As already stated in the previous paragraph these depend on the masses of the new particles, the alignment parameters $\zeta_{u,d}$ and the scalar mixing angle γ . In order to show the new physics effects, we will explicitly present the results as a quotient of the new physics prediction with the SM-EW value for the same anomalous tensor coupling.

We take the current values [27] for the standard particles. We chose different sets of values for the masses of the new neutral and charged particles; the different scenarios we consider are shown in table 2. The new scalar mass values are taken to be of the order of hundreds of GeV [37, 38]. The charged scalar mass, m_{H^+} , can take values below the top quark mass, so that the decay $t \rightarrow bH^+$ is kinematically possible and, therefore, type (c) diagrams may develop an absorptive part. These scenarios are called (i) in our paper and we take for them $m_{H^+} = 150$ GeV. For the other cases, where $m_{H^+} > m_t$, we take $m_{H^+} = 320$ GeV, as shown in table 2. In addition, for a CP conserving scalar potential [39] we have to impose that $m_h \leq m_H$. We define six different mass scenarios: two with three light neutral scalars (**I** and **Ii**), two with h as the only light scalar (**II** and **IIi**) and two more with the CP-odd scalar A being the lightest one (**III** and **IIIi**).¹

In these last scenarios we take the same mass for both neutral scalar particles (h and H). In this case, as expected, the results are independent of the mixing angle γ showing that physics cannot separate contributions from degenerate scalar mass-eigenstates. The set of scenarios given in table 2 allows us to investigate the whole meaningful parameter space and to determine the regions where the tensor couplings take values differing from the SM-EW predictions. In the scenarios (**II**), (**IIi**), (**III**) and (**IIIi**) the value of the mass of the heaviest scalar or pseudoscalar particle, 865 GeV, is fixed by setting $r_{heaviest} = (m_{heaviest})/m_t = 5$.

¹These scenarios are disfavored by present LHC data [21].

We write the alignment parameters as:

$$\varsigma_u = \rho_u e^{i\theta_u}, \quad \varsigma_d = \rho_d e^{i\theta_d}, \quad (4.1)$$

and we investigate separately the effects of modulus and phases on the anomalous tensor couplings $g_{R,L}$. Besides the masses of the new particles we have five free parameters: ρ_u , ρ_d , θ_u , θ_d and the mixing angle γ .

The deviations from the predictions of the EW sector of the SM are shown using the ratios:

$$Q_R^{\text{Re}} \equiv \frac{\text{Re}(g_R^{\text{A2HDM}})}{\text{Re}(g_R^{\text{EW}})}, \quad Q_L^{\text{Re}} \equiv \frac{\text{Re}(g_L^{\text{A2HDM}})}{\text{Re}(g_L^{\text{EW}})}, \quad (4.2)$$

$$Q_R^{\text{Im}} \equiv \frac{\text{Im}(g_R^{\text{A2HDM}})}{\text{Im}(g_R^{\text{EW}})}, \quad Q_L^{\text{Im}} \equiv \frac{\text{Im}(g_L^{\text{A2HDM}})}{\text{Im}(g_L^{\text{EW}})}. \quad (4.3)$$

These are the quotients of the real and imaginary parts of the tensor couplings calculated in the A2HDM ($g_{R,L}^{\text{A2HDM}}$) and the EW contributions of the SM to them ($g_{R,L}^{\text{EW}}$), given in eq. (3.3).

For the six different mass scenarios defined in table 2, we will show how these quotients depend on the four alignment parameters $\rho_{d,u}$, $\theta_{u,d}$, and on the mixing angle γ .

In general, we will show the results for conservative values of the modulus, i.e. for $\rho_{u,d} \sim 1$. For greater values of the modulus will certainly produce larger deviations from the SM-EW predictions.

4.1 Contributions to g_R

As a general feature we found that even for values of the modules $\rho_{u,d} \simeq 1$, the values of the anomalous tensor couplings in the A2HDM can be significantly different from the SM-EW values. We also found that the right coupling g_R is independent of the down-type alignment parameter ς_d for the same range of values as we take for ς_u ; this is due to the fact that diagrams with top quarks in the loop, specially types (b) and (d), give a big numerical contribution because the top Yukawa vertex is proportional to ς_u and to m_t . In order to fix values, we take $\rho_d = 1$ and $\theta_d = \pi/4$ to analyze the dependence of Q_R^{Re} and Q_R^{Im} on the other parameters.

In figure 2 we plot the dependence of the quotient Q_R^{Re} on the scalar mixing angle γ for the selected values of θ_u and ρ_u . It shows a smooth variation for scenarios (I) and (II), and a stronger dependence for scenarios (III) and (IIIi). As already mentioned, we found that in scenarios (III) and (IIIi) there is no dependence on γ . This is due to the fact that the two neutral scalars are degenerate in these scenarios and, then, the mixing angle has no physical content.

The real and imaginary parts of g_R have, in general, deviations from the SM-EW values of the same order of magnitude. The dependence of Q_R^{Im} on the mixing angle γ is shown in figure 3. We show the plots for $\theta_u = \pi/4$ and $\theta_u = \pi/2$ where the mass scenarios (II) and (IIIi) have great sensitivity to the angle γ .

In figure 4(a) we plot Q_R^{Re} as a function of the phase θ_u . This plot, and the ones that follows, do not strongly depend on the value of γ , and we choose $\gamma = \pi/4$ for all of them.

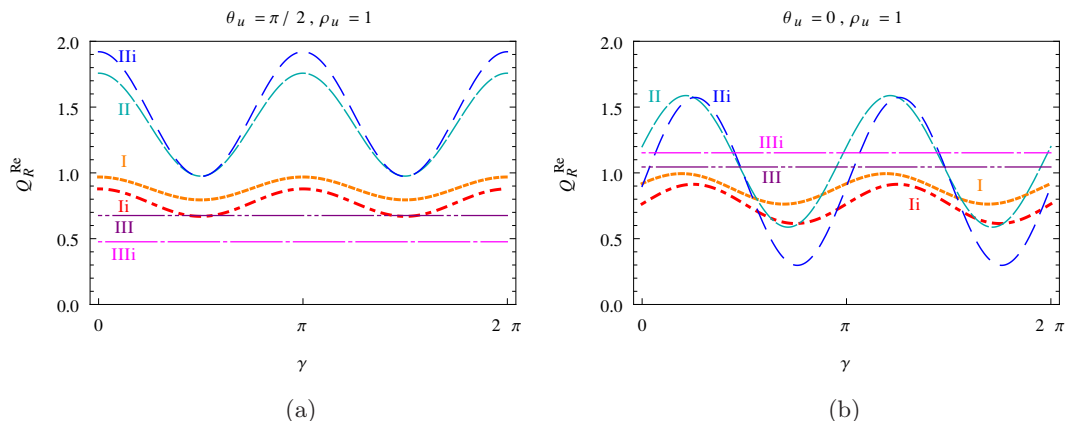


Figure 2. Plot of the quotient Q_R^{Re} as a function of γ for the different mass scenarios.

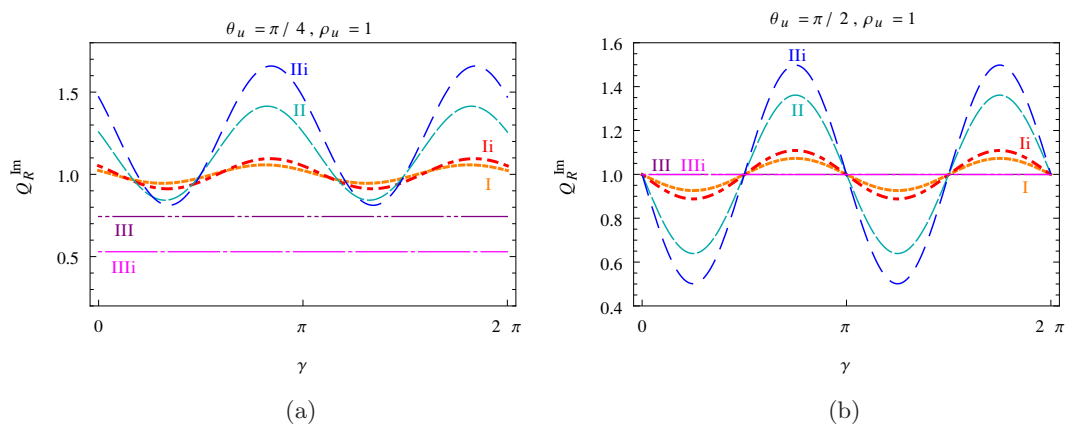


Figure 3. Plot of the quotient Q_R^{Im} as a function of γ for the different mass scenarios.

We found a strong dependence on the phase for scenarios with big scalars mass differences, being the most sensitive the ones labeled **(II)** and **(IIi)**. In the last one we found that Q_R^{Re} can even take negative values for $\theta_u \approx \pi$ when increasing the value of ρ_u up to 2. This means that $\text{Re}(g_R)$ can take positive values, contrary to the negative sign one gets in the SM-EW prediction. The dependence of Q_R^{Im} with θ_u is shown in figure 4(b), where again mass scenarios **(II)**, **(IIi)**, and **(III)**, **(IIIi)** are the most sensitive ones. In the same figure, it can be seen that if we consider the alignment parameter ς_u to be real and $\rho_u = 1$, the value of $\text{Im}(g_R)$ is the same as the one given by the EW sector of the SM, for all mass scenarios. Finally, we also obtained that when the alignment parameter ς_u is real, the dependence of Q_R^{Im} with the modulus ρ_u is almost negligible.

Figure 5 shows the dependence of Q_R^{Re} with the modulus ρ_u for all the mass scenarios we considered and for different values of θ_u . Keeping $\rho_u \lesssim 1.5$ it can be checked that, for all phases and mass scenarios, $\text{Re}(g_R)$ has the same sign as in the SM. For bigger values of ρ_u , deviations from the SM-EW value, in general, grow as ρ_u increases, but the particular behavior depends on the set of masses chosen. By the two examples shown in figure 5, it can be seen that large deviations from the SM-EW prediction (for example, bigger than 50%) can be found in almost all scenarios for $1 < \rho_u < 2$ and for any choice of the phase θ_u .

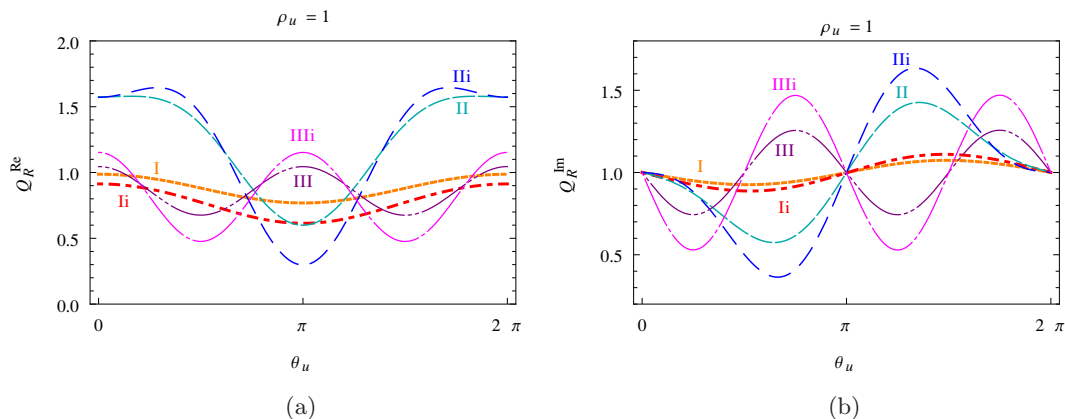


Figure 4. Plot of the quotients Q_R^{Re} and Q_R^{Im} as a function of θ_u for the different mass scenarios. We take $\gamma = \pi/4$.

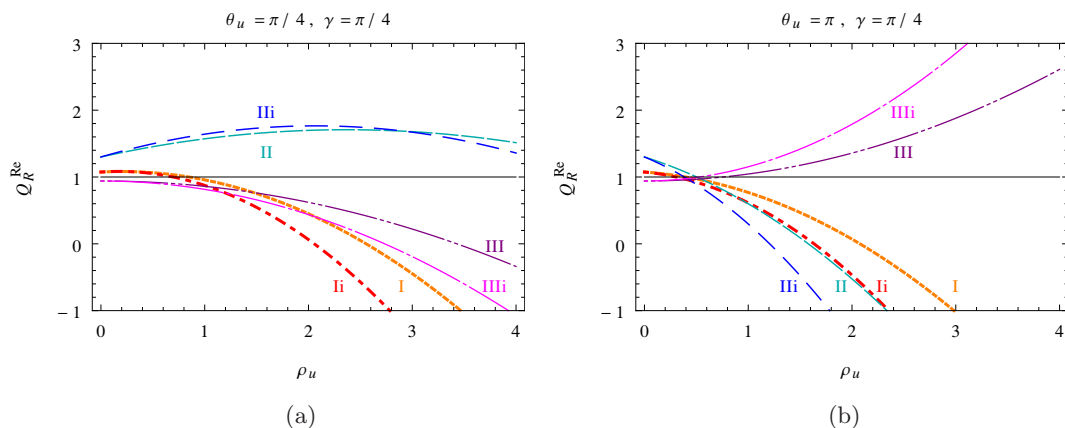


Figure 5. Plot of the quotient Q_R^{Re} as a function of ρ_u , for different mass scenarios and phases of the alignment parameters.

Figure 6 shows the dependence of Q_R^{Im} on ρ_u . We found that the Q_R^{Im} plots, as a function of ρ_u , are symmetric with respect to the $Q_R^{\text{Im}} = 1$ line when changing the phase from θ_u to $(2\pi - \theta_u)$. In figure 6(a) ($\theta_u = \pi/4$) and in figure 6(b) ($\theta_u = \pi/2$) we show that an important deviation from the EW value is obtained. However, for $\theta_u = 0$ we found a small deviation of less than five per mil from the values of the SM-EW prediction for $\text{Im}(g_R)$. This originates in the smallness of the new absorptive parts coming from the non standard contributions that are still present for $\theta_u = 0$. We also found that the deviation from the SM-EW calculation grows with ρ_u for almost all mass scenarios and for $\theta_u \neq 0$. For $\theta_u = \pi/2$ and scenarios (II) and (IIIi) this deviation can be very strong while it is negligible for scenarios (III) and (IIIi). Even if $1 < \rho_u < 2$ we still found that some scenarios (types (II) and (IIIi), for $\theta = \pi/2$, and types (III) and (IIIi), for $\theta = \pi/4$, for example) show a strong departure from the SM-EW value. We can see in figure 4(b) and figure 6 that, taking into account the current bounds on ρ_u , provided by flavor physics ($\rho_u < 2$), we still find a sizable deviation in the predicted value for $\text{Im}(g_R)$ and, therefore, for the normal asymmetry, A_{FB}^N . This result would point to a non zero complex phase θ_u and would exclude some of the mass scenarios selected.

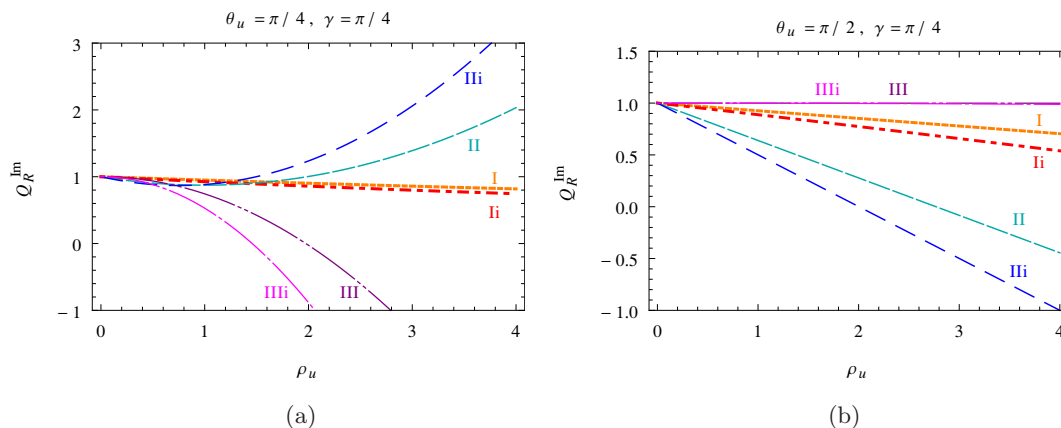


Figure 6. Plot of the quotient Q_R^{Im} as a function of ρ_u , for different mass scenarios and phases of the alignment parameters.

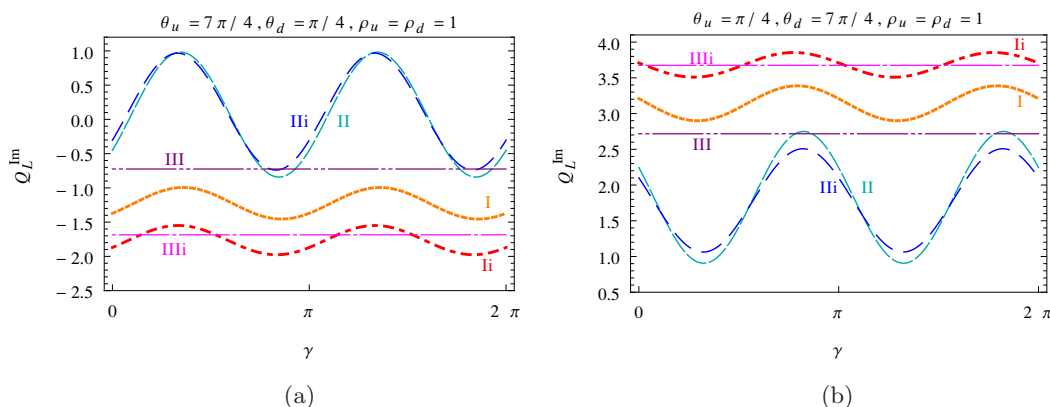


Figure 7. Plot of the quotient Q_L^{Im} as a function of γ for the different mass scenarios and phases $\theta_{u,d}$.

In general, one always can find specific mass scenarios and phases that produce sizable deviations of $\text{Im}(g_R)$ from the SM-EW value (for example, bigger than 50%). This is not the case only for $\theta_u = 0$ where there is almost no deviation from the SM-EW prediction.

4.2 Contributions to g_L

The left tensor coupling g_L depends on both alignment parameters ς_u and ς_d . The quotient Q_L^{Re} shows a soft dependence on the scalar mixing angle γ for all the mass scenarios considered, and for every $\theta_{u,d}$ combination explored. In the scenarios (III) and (IIIi) we found that, as it was the case for g_R , there is no γ -dependence at all. The oscillation of $\text{Im}(g_L)$ with the mixing angle γ is maximum when we take the phases $\theta_u + \theta_d = 2\pi$. As an example, the cases $(\theta_u = 7\pi/4, \theta_d = \pi/4)$ and $(\theta_u = \pi/4, \theta_d = 7\pi/4)$ are shown in figure 7.

The real part of the g_L coupling shows a strong dependence on the ρ_u parameter, while the dependence on the phases θ_u and θ_d is softer. This is shown in figure 8 for different values of $\theta_{u,d}$.

As can be seen from figure 8 an appreciable deviation of $\text{Re}(g_L)$ from the SM-EW value needs, in general, large values of the ρ_u parameter, such as $\rho_u > 2$. The quotient Q_L^{Re}

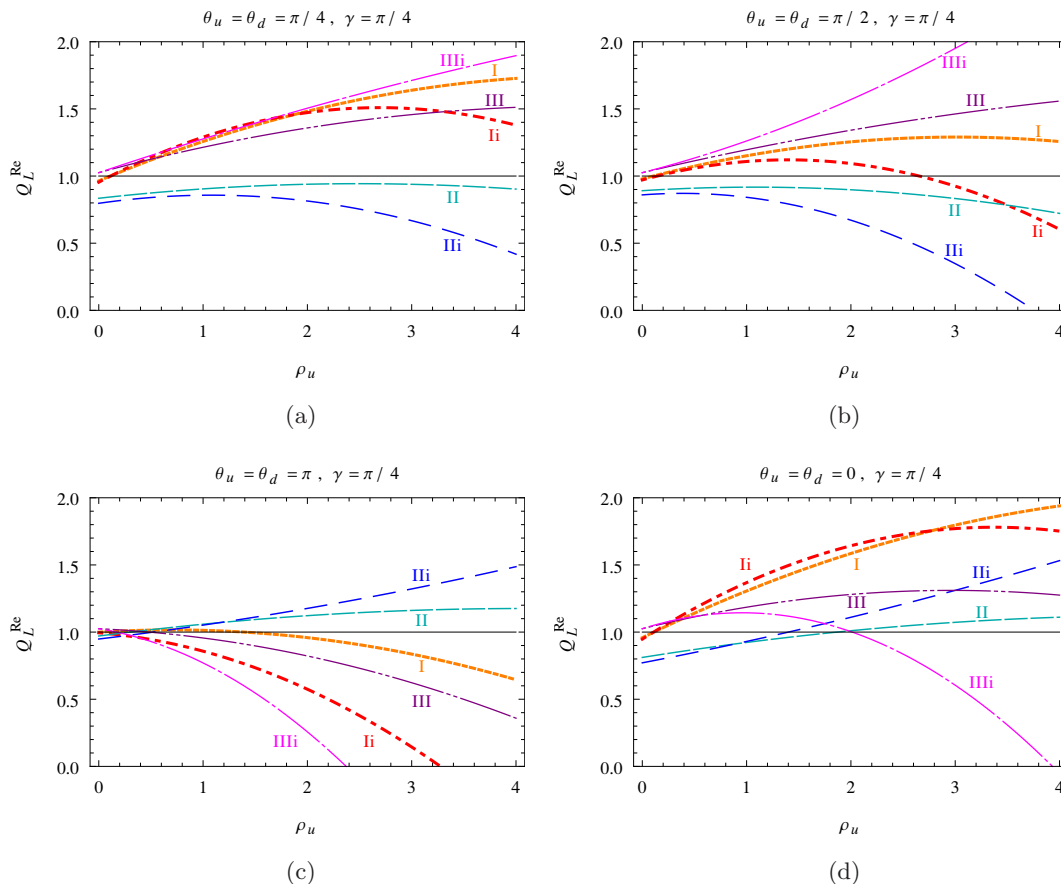


Figure 8. Plot of the quotient Q_L^{Re} as a function of ρ_u , for different mass scenarios and phases of the alignment parameters.

is always positive if $\rho_u < 2$. The current SM prediction for $\text{Re}(g_L)$ [7, 8] is slightly below the lower bound suggested in ref. [9]. This means that a positive contribution is needed in order to fit this limit. We found that the A2HDM can only accommodate that situation by taking values of $\rho_u > 2$, in tension with the current bounds given by flavor physics [17]. Only for selected phases and mass scenarios ($\theta_{u,d} = \pi$ for types (Ii) or (Iii), and $\theta_{u,d} = 0$ for types (I) or (Ii), for example) one can have deviations of the order of 50%, for $\rho_u \sim 2$.

We have also considered the dependence of Q_L^{Re} with respect to ρ_d , but no important changes result from this dependence. The quotient Q_L^{Re} has a linear dependence with ρ_d . For example, keeping $\theta_u = \theta_d$ as ρ_d grows, Q_L^{Re} exhibits a linear growing with a positive slope lower than one for every mass scenario. No important consequences are found for $\text{Re}(g_L)$ in this case and, for example, no change in the sign of $\text{Re}(g_L)$ is found with respect to the SM-EW prediction. If the phases θ_u and θ_d are taken to be in the intervals $(0, \pi)$ and $(\pi, 2\pi)$, respectively, the quotient Q_L^{Re} decreases but is always positive for every mass scenario for $\rho_d < 4$.

Figure 9 shows the strong dependence of Q_L^{Im} on the phases $\theta_{u,d}$. There it can also be seen that, due to the fact that the value of $\text{Im}(g_L)$ is very small in the SM, the quotient Q_L^{Im} is very sensitive to the $\theta_{u,d}$ phases and to the mixing angle γ . This magnitude, if measured, may allow a clear distinction between scenarios (II, Iii) and the rest of them.

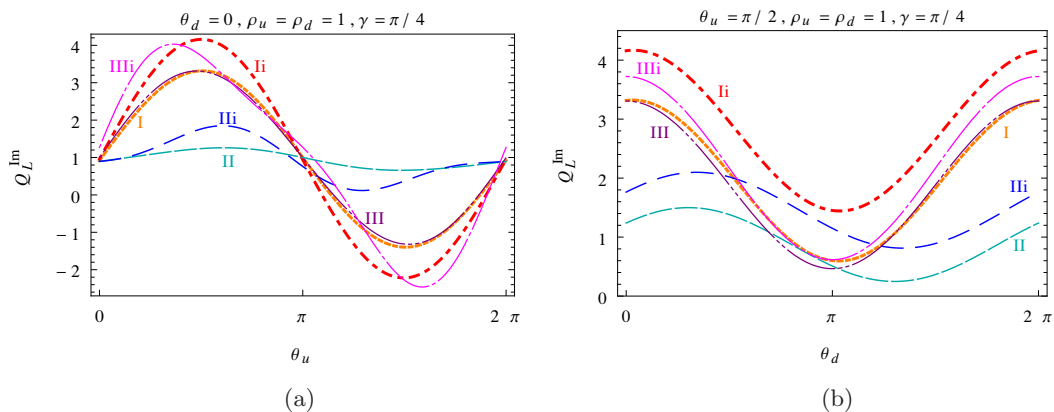


Figure 9. Plot of the quotient Q_L^{Im} as a function of θ_u and θ_d for the different mass scenarios.

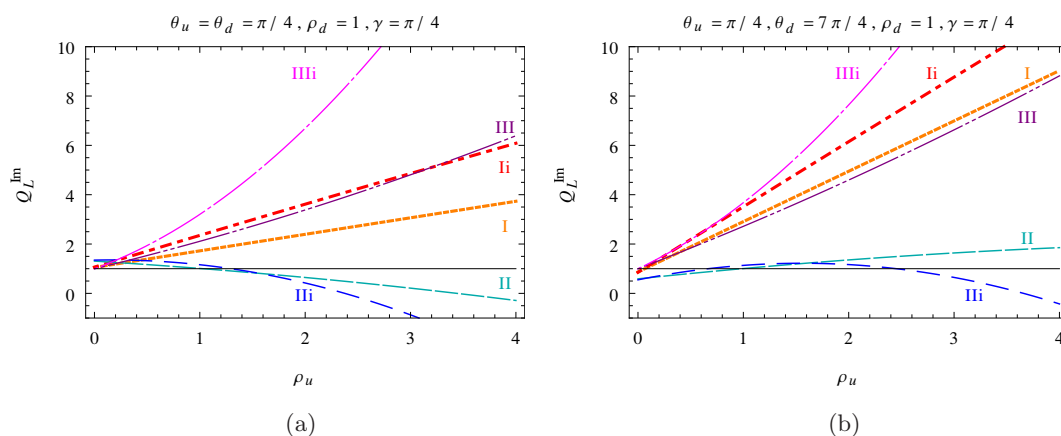


Figure 10. Plot of the quotient Q_L^{Im} as a function of ρ_u , for different mass scenarios and phases of the alignment parameters.

The Q_L^{Im} dependence on ρ_u is shown in figure 10, for different $\theta_{u,d}$ phases and taking $\rho_d = 1$. While for mass scenarios (I) and (Ii) it exhibits a linear dependence for the whole scanned ρ_u range, its dependence for scenarios (II), (IIi) and (III), (IIIi) is quadratic.

For $\theta_u = 7\pi/4$ the plots are symmetric, with respect to the $Q_L^{\text{Im}} = 1$ line, to the ones shown in figure 10. In addition, as can be seen there, deviations from the SM-EW values bigger than 100% are found for low values of the ρ_u parameter (i.e., $\rho_u < 2$). On the other hand, we have checked that $\text{Im}(g_L)$ is almost independent on ρ_u when we choose the alignment parameters to be real. In that case, the only scenarios where $\text{Im}(g_L)$ shows deviations from the SM value greater than 100% for $\rho_u < 3$ are types (IIi) and (IIIi). This is again due to new absorptive parts that are not present in the SM.

In all the mass scenarios, for $\rho_u = 1$ and for any value of the phases, we found that Q_L^{Im} grows linearly with ρ_d with positive slopes up to 1. Similarly as stated for $\text{Im}(g_R)$, a sizable deviation in the predicted value of the W helicity fraction $\rho_+ \simeq F_+/F_0$ [11, 40] would point to non zero complex phases $\theta_{u,d}$.

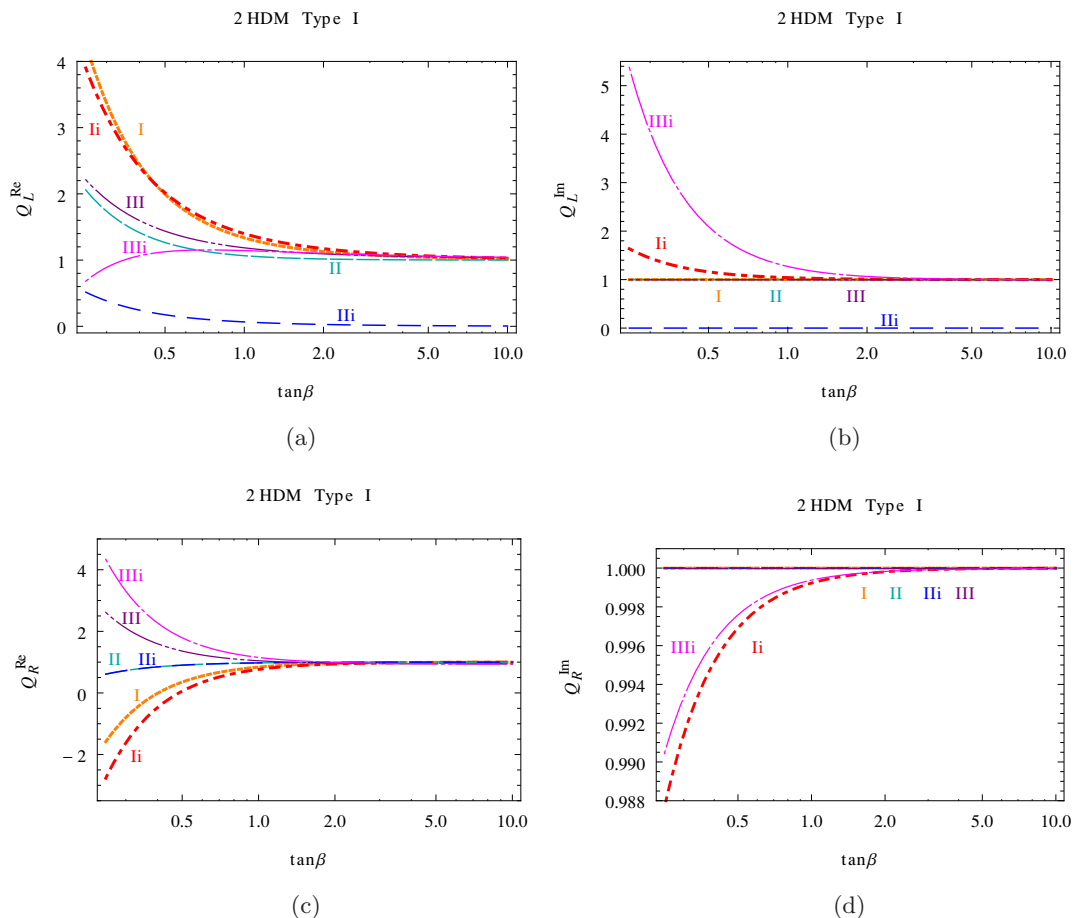


Figure 11. Plot of the quotients Q_L^{Re} , Q_L^{Im} , Q_R^{Re} and Q_R^{Im} as a function of $\tan\beta$ for the different mass scenarios in Type I 2HDM and $\beta = \alpha + \pi/2$.

4.3 Contributions from Type I and II 2HDM

For the particular case of the Type I and II 2HDM we found, taking the appropriate limit in the A2HDM parameters, the results that are shown in figure 11 and 12. As previously mentioned, Types I and II 2HDM can be recovered by choosing real alignment parameters $\varsigma_{u,d}$ [13]. The couplings in these models are usually written in a generic basis where both Higgs doublets acquire a vacuum expectation value. Then, the key parameters are the ratio of these values, parameterized as $\tan\beta = v_2/v_1$ and the mixing angle, α , between the two CP-even neutral scalars in this basis. For a CP-conserving potential we choose $\tan\beta$ and the mixing angle of the two neutral scalars h and H in such a way that $\beta = \alpha + \pi/2$. Therefore, the neutral scalar h has SM-like coupling to the photon and to the weak bosons.

Taking the alignment parameters to be $\varsigma_u = \cot\beta$ and $\varsigma_d = \cot\beta$, one recovers the Type I 2HDM, shown in figure 11. As expected, for low values of $\tan\beta$ the real parts show important deviations from the SM-EW values, and a similar behavior is found for Q_L^{Im} . The variation for Q_R^{Im} is negligible even for the type (i) scenarios.

Setting $\varsigma_u = \cot\beta$ and $\varsigma_d = -\tan\beta$ one recovers the Type II 2HDM. In figure 12 we show our results for this model. As expected, the limit $\tan\beta \gg 1$ gives singular results for

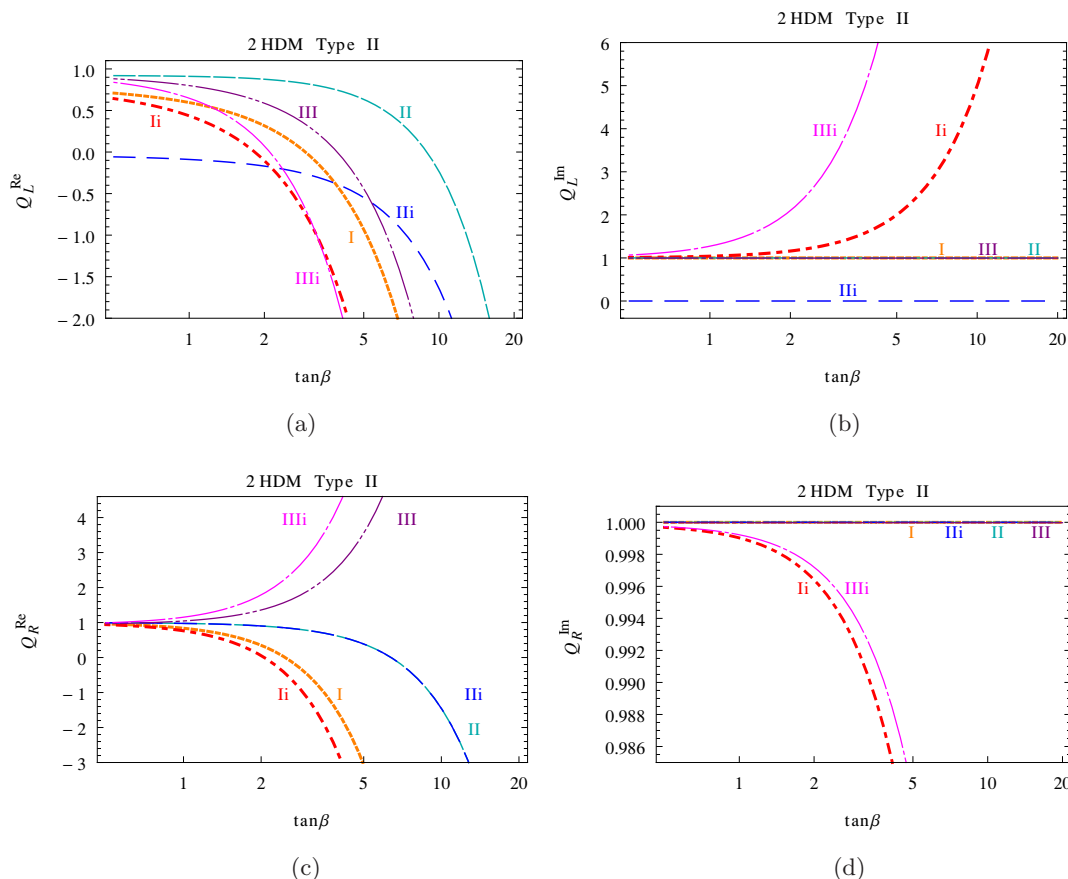


Figure 12. Plot of the quotients Q_L^{Re} , Q_L^{Im} , Q_R^{Re} and Q_R^{Im} as a function of $\tan\beta$ for the different mass scenarios in Type II 2HDM and $\beta = \alpha + \pi/2$.

the real parts in all the mass scenarios, while the imaginary part is singular in this limit only in the (Ii) and (IiIi) scenarios. The most important deviation from the SM predictions is found for Q_L^{Im} , in scenario (IiIi), dominated by the contribution of the pseudo-scalar A .

5 Conclusions

We have calculated the contributions to the top anomalous tensor couplings $g_{R,L}$ in the A2HDM with a CP-conserving potential. We have compared the numerical predictions of the model with the electroweak SM values for different scalars mass scenarios. The complete values of the couplings can be obtained by adding the QCD contribution given in eq. (3.2), to the calculated in this paper in the A2HDM.

The parameter space of the model has been extensively explored. There are large regions of this space where important deviations of the top tensor couplings from the predictions of the EW sector of the SM can be found. The four couplings $\text{Re}(g_R)$, $\text{Im}(g_R)$, $\text{Re}(g_L)$ and $\text{Im}(g_L)$ show a remarkable sensitivity to the new physics parameters and in extended regions of this parameter space they have large deviations from the EW predictions.

The study of the A2HDM in this unexplored context of top quark physics shows that the precise measurement of these magnitudes may allow for a discrimination among the different scalar mass scenarios and the value of the mixing angle γ . The measurement of the anomalous tensor couplings (real and imaginary parts) for the top quark can also reveal new CP-violation mechanisms that can be accounted for in the A2HDM by the complex alignment parameters $\varsigma_{u,d}$. The observables considered in the literature, taken together with the results presented in this paper can help in finding new physics and also in restricting the range of the allowed regions of the parameter space in the A2HDM.

As expected, the right coupling g_R is not sensitive to the down alignment parameter ς_d . The dependence of the real part $\text{Re}(g_R)$ with ρ_u allows to discriminate between different scalar mass scenarios. Taking into account the constraint $\rho_u < 2$, coming from B physics, one can also have deviations from the SM-EW prediction up to 100%. This means that the contribution of the A2HDM to $\text{Re}(g_R)$ can, by itself, make this number a 15% higher than the SM prediction. These large effects can even change the sign of the A2HDM contribution to the top couplings with respect to the electroweak SM prediction for different values of θ_u . Despite not being the most sensitive quantity to the value of the new physics parameters, the quotient Q_R^{Im} can take values from 0.5 up to 1.5, for $\rho_u = 1$ and for several values of θ_u . We also have found that the absorptive parts are less than 5% of the electroweak SM value even for high values of ρ_u (i.e. $\rho_u \simeq 4$), for a pure real alignment parameter ς_u . $\text{Im}(g_R)$ has already been measured at the LHC [6], taking advantage of the recently investigated asymmetries in the normal direction [11], and future measurements may show sensitivity to new physics. A significant deviation of this measurement from the electroweak SM value would point to new CP-violation mechanisms such as the non-zero phases $\theta_{u,d}$.

The left anomalous tensor coupling g_L shows sizable dependencies on both alignment parameters, and both the real and imaginary parts are very sensitive to these parameters. For $\text{Re}(g_L)$ there are some values of the ρ_u parameter where this magnitude can change sign with respect to the electroweak SM prediction. Then, the total one loop QCD plus A2HDM prediction for this coupling is 18% lower than the SM one given in eq. (3.4). Besides, this fact could produce contributions that may elucidate the tension between the indirect bounds put on $\text{Re}(g_L)$ by $b \rightarrow s\gamma$ decays and the SM prediction. The imaginary part of g_L is extremely sensitive to ρ_u and to both complex phases $\theta_{u,d}$. We have found that it can deviate from the SM prediction up to 400%, even for low values of the ρ_u parameter ($\simeq 1$).

In both Type I and II models we found that the real parts have important deviations from the EW values. The imaginary parts of the couplings also have sizable deviations from the electroweak SM predictions in some of the studied mass scenarios. For the Type I models and for low values of $\tan\beta$ we found that the real parts deviate strongly from the EW prediction, while this only occurs in some of the scenarios for the imaginary part. The limit $\tan\beta \gg 1$ gives singular results for the real parts in Type II models in all the scenarios, while the imaginary part is singular in this limit in scenarios (II) and (III).

High precision measurements of the top quark anomalous tensor couplings are expected in the next high energy runs at the LHC and in the next generation of colliders. These measurements, the flavor constraints and the collider searches for new scalar resonances are complementary insights and will illuminate this up to now almost unexplored physics.

Acknowledgments

This work has been supported, in part, by the Ministerio de Ciencia e Innovación, Spain, under grants FPA2011-23897 and FPA2011-23596; by Generalitat Valenciana, Spain, under grant PROMETEO/2009/128; and by Pedeciba, CSIC, and ANII under grant BE-POS-2010-2260 and PR-FCE-2009-1-2986, Uruguay.

References

- [1] ATLAS collaboration, *Observation of a new particle in the search for the standard model Higgs boson with the ATLAS detector at the LHC*, *Phys. Lett. B* **716** (2012) 1 [[arXiv:1207.7214](#)] [[INSPIRE](#)].
- [2] CMS collaboration, *Observation of a new boson at a mass of 125 GeV with the CMS experiment at the LHC*, *Phys. Lett. B* **716** (2012) 30 [[arXiv:1207.7235](#)] [[INSPIRE](#)].
- [3] D0 collaboration, V.M. Abazov et al., *Measurement of the W boson helicity in top quark decays using 5.4 fb⁻¹ of p \bar{p} collision data*, *Phys. Rev. D* **83** (2011) 032009 [[arXiv:1011.6549](#)] [[INSPIRE](#)].
- [4] ATLAS collaboration, *Measurement of the W boson polarization in top quark decays with the ATLAS detector*, *JHEP* **06** (2012) 088 [[arXiv:1205.2484](#)] [[INSPIRE](#)].
- [5] CMS collaboration, *Measurement of the W-boson helicity in top-quark decays from t \bar{t} production in lepton+jets events in pp collisions at $\sqrt{s} = 7$ TeV*, *JHEP* **10** (2013) 167 [[arXiv:1308.3879](#)] [[INSPIRE](#)].
- [6] ATLAS collaboration, *Search for CP violation in single top quark events in pp collisions at $\sqrt{s} = 7$ TeV with the ATLAS detector*, *ATLAS-CONF-2013-032* (2013).
- [7] G.A. González-Sprinberg, R. Martinez and J. Vidal, *Top quark tensor couplings*, *JHEP* **07** (2011) 094 [*Erratum ibid.* **1305** (2013) 117] [[arXiv:1105.5601](#)] [[INSPIRE](#)].
- [8] G.A. González-Sprinberg, R. Martinez and J. Vidal, *Top quark tensor couplings*, *JHEP* **07** (2011) 094 [*Erratum ibid.* **1305** (2013) 117] [[arXiv:1105.5601](#)] [[INSPIRE](#)].
- [9] J. Drobnak, S. Fajfer and J.F. Kamenik, *Probing anomalous tWb interactions with rare B decays*, *Nucl. Phys. B* **855** (2012) 82 [[arXiv:1109.2357](#)] [[INSPIRE](#)].
- [10] B. Grzadkowski and M. Misiak, *Anomalous Wtb coupling effects in the weak radiative B-meson decay*, *Phys. Rev. D* **78** (2008) 077501 [*Erratum ibid.* **D 84** (2011) 059903] [[arXiv:0802.1413](#)] [[INSPIRE](#)].
- [11] J. Aguilar-Saavedra and J. Bernabeu, *W polarisation beyond helicity fractions in top quark decays*, *Nucl. Phys. B* **840** (2010) 349 [[arXiv:1005.5382](#)] [[INSPIRE](#)].
- [12] G. Branco et al., *Theory and phenomenology of two-Higgs-doublet models*, *Phys. Rept.* **516** (2012) 1 [[arXiv:1106.0034](#)] [[INSPIRE](#)].
- [13] A. Pich and P. Tuzon, *Yukawa alignment in the two-Higgs-doublet model*, *Phys. Rev. D* **80** (2009) 091702 [[arXiv:0908.1554](#)] [[INSPIRE](#)].
- [14] M. Beneke et al., *Top quark physics*, [hep-ph/0003033](#) [[INSPIRE](#)].
- [15] T.M. Tait and C.-P. Yuan, *Single top quark production as a window to physics beyond the standard model*, *Phys. Rev. D* **63** (2000) 014018 [[hep-ph/0007298](#)] [[INSPIRE](#)].

- [16] W. Bernreuther, P. Gonzalez and M. Wiebusch, *The top quark decay vertex in standard model extensions*, *Eur. Phys. J. C* **60** (2009) 197 [[arXiv:0812.1643](#)] [[INSPIRE](#)].
- [17] M. Jung, A. Pich and P. Tuzon, *Charged-Higgs phenomenology in the aligned two-Higgs-doublet model*, *JHEP* **11** (2010) 003 [[arXiv:1006.0470](#)] [[INSPIRE](#)].
- [18] M. Jung, A. Pich and P. Tuzon, *The $B \rightarrow Xs\gamma$ rate and CP asymmetry within the aligned two-Higgs-doublet model*, *Phys. Rev. D* **83** (2011) 074011 [[arXiv:1011.5154](#)] [[INSPIRE](#)].
- [19] M. Jung, X.-Q. Li and A. Pich, *Exclusive radiative B-meson decays within the aligned two-Higgs-doublet model*, *JHEP* **10** (2012) 063 [[arXiv:1208.1251](#)] [[INSPIRE](#)].
- [20] A. Celis, M. Jung, X.-Q. Li and A. Pich, *Sensitivity to charged scalars in $B \rightarrow D^{(*)}\tau\nu_\tau$ and $B \rightarrow \tau\nu_\tau$ decays*, *JHEP* **01** (2013) 054 [[arXiv:1210.8443](#)] [[INSPIRE](#)].
- [21] A. Celis, V. Ilisie and A. Pich, *LHC constraints on two-Higgs doublet models*, *JHEP* **07** (2013) 053 [[arXiv:1302.4022](#)] [[INSPIRE](#)].
- [22] BABAR collaboration, J. Lees et al., *Evidence for an excess of $\bar{B} \rightarrow D^{(*)}\tau^-\bar{\nu}_\tau$ decays*, *Phys. Rev. Lett.* **109** (2012) 101802 [[arXiv:1205.5442](#)] [[INSPIRE](#)].
- [23] CDF, D0 collaboration, T. Aaltonen et al., *Evidence for a particle produced in association with weak bosons and decaying to a bottom-antibottom quark pair in Higgs boson searches at the Tevatron*, *Phys. Rev. Lett.* **109** (2012) 071804 [[arXiv:1207.6436](#)] [[INSPIRE](#)].
- [24] W. Buchmüller and D. Wyler, *Effective lagrangian analysis of new interactions and flavor conservation*, *Nucl. Phys. B* **268** (1986) 621 [[INSPIRE](#)].
- [25] J. Aguilar-Saavedra, *A minimal set of top anomalous couplings*, *Nucl. Phys. B* **812** (2009) 181 [[arXiv:0811.3842](#)] [[INSPIRE](#)].
- [26] G.L. Kane, G. Ladinsky and C. Yuan, *Using the top quark for testing standard model polarization and CP predictions*, *Phys. Rev. D* **45** (1992) 124 [[INSPIRE](#)].
- [27] PARTICLE DATA GROUP collaboration, J. Beringer et al., *Review of particle physics*, *Phys. Rev. D* **86** (2012) 010001 [[INSPIRE](#)].
- [28] C.S. Li, R.J. Oakes and T.C. Yuan, *QCD corrections to $t \rightarrow W^+b$* , *Phys. Rev. D* **43** (1991) 3759 [[INSPIRE](#)].
- [29] B. Lampe, *Forward-backward asymmetry in top quark semileptonic decay*, *Nucl. Phys. B* **454** (1995) 506 [[INSPIRE](#)].
- [30] F. del Aguila and J. Aguilar-Saavedra, *Precise determination of the Wtb couplings at CERN LHC*, *Phys. Rev. D* **67** (2003) 014009 [[hep-ph/0208171](#)] [[INSPIRE](#)].
- [31] S.D. Rindani and P. Sharma, *Probing anomalous tbW couplings in single-top production using top polarization at the Large Hadron Collider*, *JHEP* **11** (2011) 082 [[arXiv:1107.2597](#)] [[INSPIRE](#)].
- [32] D0 collaboration, V.M. Abazov et al., *Combination of searches for anomalous top quark couplings with 5.4 fb^{-1} of $p\bar{p}$ collisions*, *Phys. Lett. B* **713** (2012) 165 [[arXiv:1204.2332](#)] [[INSPIRE](#)].
- [33] D0 collaboration, V.M. Abazov et al., *Search for anomalous Wtb couplings in single top quark production in $p\bar{p}$ collisions at $\sqrt{s} = 1.96 \text{ TeV}$* , *Phys. Lett. B* **708** (2012) 21 [[arXiv:1110.4592](#)] [[INSPIRE](#)].
- [34] J. Aguilar-Saavedra, N. Castro and A. Onofre, *Constraints on the Wtb vertex from early LHC data*, *Phys. Rev. D* **83** (2011) 117301 [[arXiv:1105.0117](#)] [[INSPIRE](#)].

- [35] Z. Ligeti, M. Papucci, G. Perez and J. Zupan, *Implications of the dimuon CP asymmetry in $B_{d,s}$ decays*, *Phys. Rev. Lett.* **105** (2010) 131601 [[arXiv:1006.0432](#)] [[INSPIRE](#)].
- [36] A. Lenz et al., *Anatomy of new physics in B - \bar{B} mixing*, *Phys. Rev. D* **83** (2011) 036004 [[arXiv:1008.1593](#)] [[INSPIRE](#)].
- [37] CDF collaboration, T. Aaltonen et al., *Search for a Higgs boson in the diphoton final state in $p\bar{p}$ collisions at $\sqrt{s} = 1.96$ TeV*, *Phys. Rev. Lett.* **108** (2012) 011801 [[arXiv:1109.4427](#)] [[INSPIRE](#)].
- [38] D0 collaboration, V. Abazov et al., *Search for the standard model and a fermiophobic Higgs boson in diphoton final states*, *Phys. Rev. Lett.* **107** (2011) 151801 [[arXiv:1107.4587](#)] [[INSPIRE](#)].
- [39] J.F. Gunion, H.E. Haber, G.L. Kane and S. Dawson, *The Higgs hunter's guide*, *Front. Phys.* **80** (2000) 1 [[INSPIRE](#)].
- [40] J. Aguilar-Saavedra, J. Carvalho, N.F. Castro, A. Onofre and F. Veloso, *ATLAS sensitivity to Wtb anomalous couplings in top quark decays*, *Eur. Phys. J. C* **53** (2008) 689 [[arXiv:0705.3041](#)] [[INSPIRE](#)].